Electroreduction of Carbon Dioxide to Acetate using Heterogenized Hydrophilic Manganese Porphyrins

Abdinejad, Maryam; Yuan, Tiange; Tang, Keith; Duangdangchote, Salatan; Iglesias van Montfort, Hugo Pieter; Li, Mengran; Middelkoop, Joost; Wolff, Mädchen; Burdyny, Thomas; More Authors

DOI
10.1002/chem.202203977

Publication date
2023

Document Version
Final published version

Published in
Chemistry - A European Journal

Chemistry Europe
European Chemical Societies Publishing

WILEY VCH

Excellence in Chemistry Research

Announcing our new flagship journal

- Gold Open Access
- Publishing charges waived
- Preprints welcome
- Edited by active scientists

Meet the Editors of *ChemistryEurope*

Luisa De Cola
Università degli Studi di Milano Statale, Italy

Ive Hermans
University of Wisconsin-Madison, USA

Ken Tanaka
Tokyo Institute of Technology, Japan

Chemistry–A European Journal
Research Article
doi.org/10.1002/chem.202203977
Chemistry Europe
European Chemical Societies Publishing
www.chemeurj.org

Electroreduction of Carbon Dioxide to Acetate using Heterogenized Hydrophilic Manganese Porphyrins

Maryam Abdinejad[+],*[a] Tiange Yuan[+],[b] Keith Tang,[b] Salatan Duangdangchote,[b] Amirhossein Farzi,[c] Hugo-Pieter Iglesias van Montfort,[a] Mengran Li,[a] Joost Middelkoop,[a] Mädchen Wolff,[a] Ali Seifitokaldani,[c] Oleksandr Voznyy,*[b] and Thomas Burdyny*[a]

Abstract: The electrochemical reduction of carbon dioxide (CO_2) to value-added chemicals is a promising strategy to mitigate climate change. Metalloporphyrins have been used as a promising class of stable and tunable catalysts for the electrochemical reduction reaction of CO_2 (CO_2RR) but have been primarily restricted to single-carbon reduction products. Here, we utilize functionalized earth-abundant manganese tetraphenylporphyrin-based (Mn-TPP) molecular electrocatalysts that have been immobilized via electrografting onto a glassy carbon electrode (GCE) to convert CO_2 with overall 94% Faradaic efficiencies, with 62% being converted to acetate. Tuning of Mn-TPP with electron-withdrawing sulfonate groups (Mn-TPPS) introduced mechanistic changes arising from the electrostatic interaction between the sulfonate groups and water molecules, resulting in better surface coverage, which facilitated higher conversion rates than the non-functionalized Mn-TPP. For Mn-TPP only carbon monoxide and formate were detected as CO_2 reduction products. Density-functional theory (DFT) calculations confirm that the additional sulfonate groups could alter the C–C coupling pathway from *CO→*COH→*COH-CO to *CO→*CO-CO→*COH-CO, reducing the free energy barrier of C–C coupling in the case of Mn-TPPS. This opens a new approach to designing metalloporphyrin catalysts for two carbon products in CO_2RR.

Introduction

Electrochemical carbon dioxide (CO_2) reduction reactions (CO_2RRs) in aqueous solutions is a promising approach to address pressing matters of CO_2 emissions from non-renewable fuel sources.[1,2] Challenges to CO_2 efforts arise due to the high stability of the C=O chemical bond[3] and the competition of hydrogen evolution reactions (HERs), creating a tight bottleneck on the effective implementation of these technologies.[4] As a consequence, catalytic systems designed to overcome high activation energy barriers are in demand. Several electrocatalysts driving CO_2RR have been reported ranging from transition metal catalysts[5–8] to molecular complexes,[9,10] in both homogeneous and heterogeneous capacities.[11,12] Although homogeneous systems offer a simple and cost-effective method to quickly screen potential molecular complexes,[13] the recyclability of heterogeneous systems make them the de facto approach to CO_2 conversion.[14]

Heterogenization through the immobilization of molecular electrocatalysts onto conductive surfaces has resulted in efficient systems that show an increase in current density (*j*) and a reduction in applied overpotentials.[14,15] Electrografting of molecular catalysts onto electrode surfaces[16,17] is an effective method to incorporate homogeneous molecules onto a heterogeneous surface and offers the benefit of control over their steric and electronic properties.[18,19] Among organometallic catalysts, metalloporphyrins are attractive due to their stability, selectivity, and tunability.[20-23] The metal ion resting in the porphyrin cavity acts as an electron-transfer (ET) mediator as well as the CO_2 capture site.[24] In addition, tunability of the porphyrin electronic environment can be achieved through facile manipulation of peripheral ligand structures, allowing for direct control over their catalytic activity.[25] The majority of studies on metalloporphyrin systems focus only on one-carbon (C_1) products, such as CO and formate, and the potential for two carbon reduction products (C_2) remains obscure.

While others have reported several metallated porphyrins[26] with a variety of metal centers such as Fe,[27,28] Co,[29–31] Ni,[32] Zn,[33] etc. Manganese (Mn)-based porphyrins are scarcely

[a] *M. Abdinejad,[+] H.-P. Iglesias van Montfort, M. Li, J. Middelkoop, M. Wolff, Prof. T. Burdyny*
Department of Chemical Engineering
Delft University of Technology
Van der Maasweg 9 2629 HZ Delft (the Netherlands)
E-mail: M.Abdinejad@tudelft.nl
T.E.Burdyny@tudelft.nl

[b] *T. Yuan,[+] K. Tang, S. Duangdangchote, Prof. O. Voznyy*
Department of Physical and Environmental Sciences
University of Toronto
1265 Military Trail, Toronto, ON M1 C 1 A4 (Canada)
E-mail: o.voznyy@utoronto.ca

[c] *A. Farzi, A. Seifitokaldani*
Department of Chemical Engineering
McGill University
3610 University Street, Montréal, H3 A 0 C5 QC (Canada)

[+] *These authors contributed equally to this work.*

Supporting information for this article is available on the WWW under https://doi.org/10.1002/chem.202203977

reported for electrochemical CO_2RR. Compared with Fe–N–C and Ni–N–C catalysts, the electrocatalytic activity of Mn-N–C remains a subject of interest.[34,35] It's been shown that an Mn-based molecular catalyst can reduce CO_2 to acetate with a Faradaic efficiency (FE) of 63% and a current density of -0.8 mA/cm^2 at -0.67 V vs. RHE.[36] Aleksei et al.,[37] observed that tuning the Mn–Mn distance of electrografted Mn-porphyrins promoted the number of electron transfers between the two porphyrin metal centers. In this work, we designed and investigated the electrocatalytic activity of a manganese-*meso*-tetrakis (*p*-sulfonyl phenyl) porphyrin (Mn-TPPS) compound for the electroreduction of CO_2 in a heterogeneous capacity via an electrografting technique.[16,17]

We hypothesized that: i) the coordination of negatively charged sulfonate ($-SO_3^-$) groups in *para* positions with water molecules will tune through-structure effects via electrostatic attraction;[38,39] ii) sulfonate substituents with electron-withdrawing functionalities lower the overpotential of CO_2 reduction and facilitate C–O bond cleavage;[40,41] iii) the tunability of the Mn–Mn distance can be leveraged to facilitate the electron transfer between the Mn-porphyrin centers hence improve the current density; and iv) the vertical molecular geometry of the immobilized molecules can stabilize key product intermediates (e.g., *HOCO to *CO) and promote the chance of C–C coupling towards C_2 products.

To thoroughly examine this hypothesis and highlight the role of sulfonate groups, the electrochemical activity of the Mn-TPPS towards CO_2RR will be reported along with its non-substituted and non-polar analogue (Mn-TPP) shown in Figure 1. Compound Mn-TPP displayed an overall FE of 55% with a current density of -1.22 mA/cm^2 at -1.0 V vs. RHE. Where Mn-TPPS displayed significant improvement in the overall FE of 94% and current density of -6.1 mA/cm^2 with a positive shift in potential to -0.8 V vs. RHE (Table S1). Density functional theory (DFT) calculations investigating the C–C coupling step reveals electronic interaction between the metal centers of the Mn-TPPS structure, showing reduced reaction barriers towards acetate versus Mn-TPP.

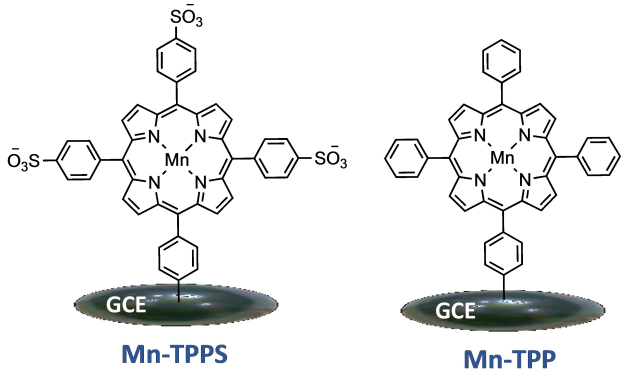

Figure 1. Molecular structure of heterogeneous Mn-TPPS and Mn-TPP electrocatalysts immobilized on glassy carbon electrodes (GCE).

Results and Discussion

Synthesis, characterization, and heterogenization of manganese porphyrins on electrode surface

As shown in Scheme S1, the porphyrin derivatives were synthesized as reported previously with a minor modification.[42–45] The proton nuclear magnetic resonance (^{1}H NMR) shows characteristic information of A_3B type of TPP analogue, as indicated by the asymmetry (multiplet) in the β-pyrrole H peaks (Figure S1-S2).[46] Due to the high molar absorption coefficient of porphyrin molecules in the UV–Visible (UV-Vis) region, spectral properties are particularly important to the characterization of the porphyrin and metalloporphyrin species. The UV-Vis absorption spectra comparison in Figure S3 shows characteristic peaks of porphyrin complexes, including a Soret absorption peak at 419 nm, and four Q bands at 513 nm, 555 nm, 589 nm and 648 nm in the case of TPP-NH_2,[47] which blue shifted to a λ_{max} of 415 nm after sulfonation (TPPS).

The main steps of covalent immobilization of TPPS-NH_2 on the glassy carbon electrode surface, followed by the metalation process are depicted in Figure 2a. The diazonium porphyrin salt is produced through diazotation of the amino porphyrin (TPP-NH_2) using $NaNO_2$ (2 mM) and HCl (0.5 M) to form TPP-N_2 (SI-Part S4).[48] Once the diazotation reaction was completed, the diazonium cation was reduced on the glassy carbon electrode in situ between 0 to -0.8 v vs. Ag/AgCl using three cycles of cyclic voltammogram at a scan rate of 50 mV/s shown in Figure 2b,[49,50] followed by metalation using 0.05 M solution of $MnCl_2$ in DMF at 120 °C to form Mn-TPPS, consistent with literature reports.[51] Next, the electrode was sonicated in 20 mL pure DMF for 30 min, followed by another 30 min sonication in water and rinsing. The same method was used for the non-substituted Mn-TPP (Figure S4).

The chemical, structural information, and surface characterization of the electrografted porphyrins were examined and monitored during the reaction using X-ray photoelectron spectra (XPS). The full XPS survey scan shows the characteristic binding energy regions corresponding to Mn 2p, O 1s, C 1s, N 1s, and S2p, proving the presence of those elements, hence successful immobilization of the compounds onto the electrode surface (Figure 2c). The N 1s at 399.2 eV is related to four N species, including Mn–N pyrrolic N species at 398.0 eV, pyrrolic N species at 400.7 eV and graphitic N species at 401.5 eV.[34,35] The spectra of Mn 2p exhibit two distinct peaks centered on 642.4 and 654.5 eV, corresponding to Mn $2p^{3/2}$ and Mn $2p^{1/2}$, respectively. The peak at 530.7 eV indicates that O is present in the O^{2-} state and binds with Mn atoms.[52,53] The XPS measurements were also performed after CO_2 electrolysis, which confirms that the peaks for Mn 2p, C 1s, N 1s and S2p are positioned at the same energy regions confirming the stability of the catalysts (Figure S6).

Using a ferricyanide redox probe (aqueous 2.5 mM $K_3Fe(CN)_6$/200 mM KNO_3), a clear suppression of current density was observed after electrografting, which indicates the successful formation of the organic layer on the electrode surface

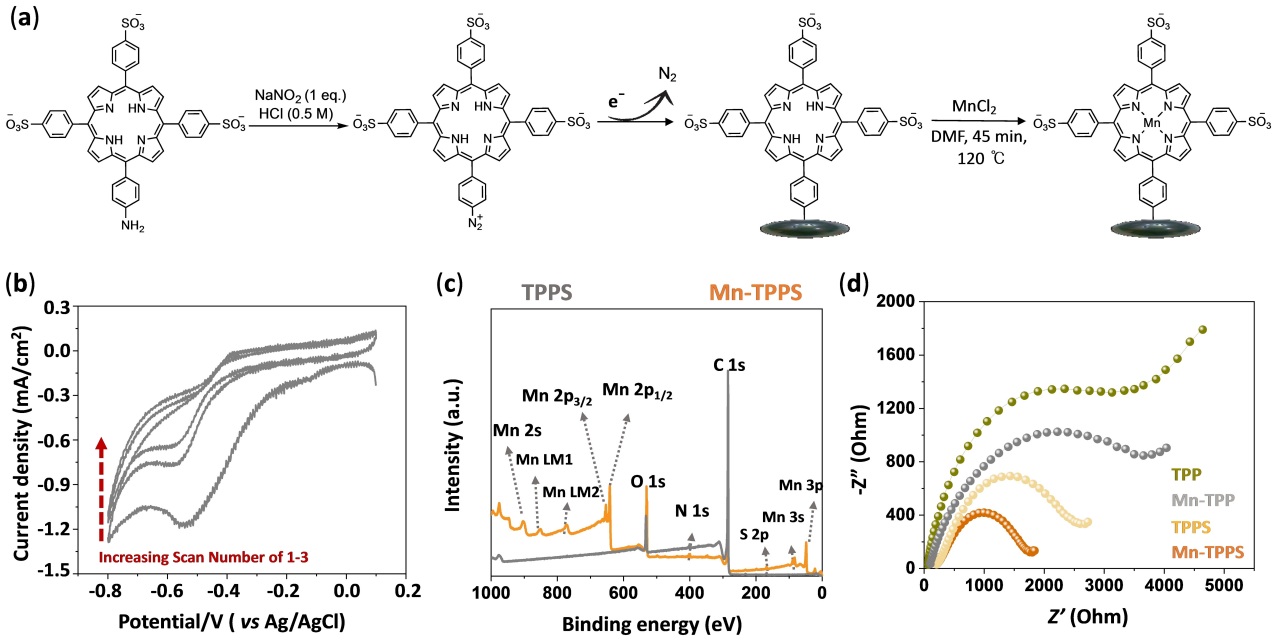

Figure 2. (a) Electrografting of non-metallated porphyrin (TPPS-NH_2) reaction on a glassy carbon electrode (GCE) followed by metal insertion process to form Mn-TPPS; (b) Electrografting voltammogram of 5 mM TPPS in 2 mM $NaNO_2$ in 0.5 M HCl at a scan rate of 50 mV/s; (c) X-ray photoelectron spectroscopy (XPS) survey spectra comparison of immobilized TPPS and Mn-TPPS in 2.5 mM $[Fe(CN)_6]^{3-/4-}$ and 0.2 M KNO_3; and (d) Nyquist diagrams of TPP, Mn-TPP, TPPS, and Mn-TPPS in 2.5 mM $[Fe(CN)_6]^{3-/4-}$ and 0.2 M KNO_3.

(Figure S5).[54] The decrease in the current density of the probe's redox profile before and after molecular deposition, which indicates the lower access of the probe to the electrode due to the formation of the porphyrin layer on the electrode surface.[48] To further evaluate the metal center and SO_3^- substituents effect on the electron distribution, Electrochemical impedance spectroscopy (EIS) was applied on both metallated and non-metallated heterogeneous porphyrin using a 2.5 mmol $K_3Fe(CN)_6$ redox probe in 0.2 M KNO_3 solution (Figure 2d). The Nyquist plots in Figure 2d show TPP (3545.1 ± 31.5 Ω) with the largest charge transfer resistance (R_{ct}) followed by Mn-TPP (3507 ± 72.1 Ω), TPPS (2581 ± 39.6 Ω) and Mn-TPPS (1726 ± 31.4 Ω), respectively. The lowest R_{ct} in the case of Mn-TPPS, suggests a favorable Faradaic process, which is evidence of the improvement in electrical conductivity the metal center and sulfonate groups offer.[55]

The surface concentration (Γ) of both Mn-TPPS and Mn-TPP was calculated according to Equation (1).

$$\Gamma = \frac{Q}{nFA} \quad (1)$$

where Q is the total charge, n is the number of electrons transferred (1e⁻), F is the Faraday constant (96485 C/mol), and A is the electrode surface area (0.071 cm^2). The total charge was obtained by integrating the first electrografting CV peak. The surface concentration of the electrografted Mn-TPPS and Mn-TPP was calculated as 3.5 x 10^{-9} mol/cm^2 and 6.5 x 10^{-11} mol/cm^2, respectively. A ~50-fold increase in the Mn-TPPS molecular catalyst deposited on the electrode surface can be attributed to the electrostatic coordination of the sulfonate group in Mn-TPPS with water molecules, hence better surface coverage, which allows the molecular catalyst to be more homogenously dispersed during deposition.

To further investigate the surface area rate of electron transfer between the Mn-porphyrins and electrode surface in both cases, the electroreduction of CO_2 of Mn-TPP and Mn-TPPS were evaluated at various scan rates of 20, 40, 60, 80 and 100 mV/s (Figure S7a and S7b). A linear relationship between the reduction peak currents and the square root of the scan rate ($v^{1/2}$) was observed.[56] According to the measured electrochemical surface area (ECSA) in Figure S7c, the ECSA for Mn-TPPS (0.164 cm^2) is higher than Mn-TPP (0.058 cm^2), which indicates that Mn-TPPS offers a more accessible charge surface in the electrolytic process which could be due to better synergistic interaction with the electrode and Mn-TPPS molecules.

Electrochemical characterization of heterogeneous Mn-porphyrins towards CO_2RR

Electrocatalytic CO_2RR activity of the heterogeneous synthesized porphyrin derivatives was evaluated in 0.1 M $KHCO_3$ in a two-compartment H-cell electrolyzer. A three-electrode, sealed system including a modified glassy carbon working electrode, platinum counter electrode and silver chloride (Ag/AgCl) reference electrode was employed. The CV comparison of Mn-TPP and Mn-TPPS in Figure 3a clearly shows a dramatic enhancement of current density upon saturation of solution

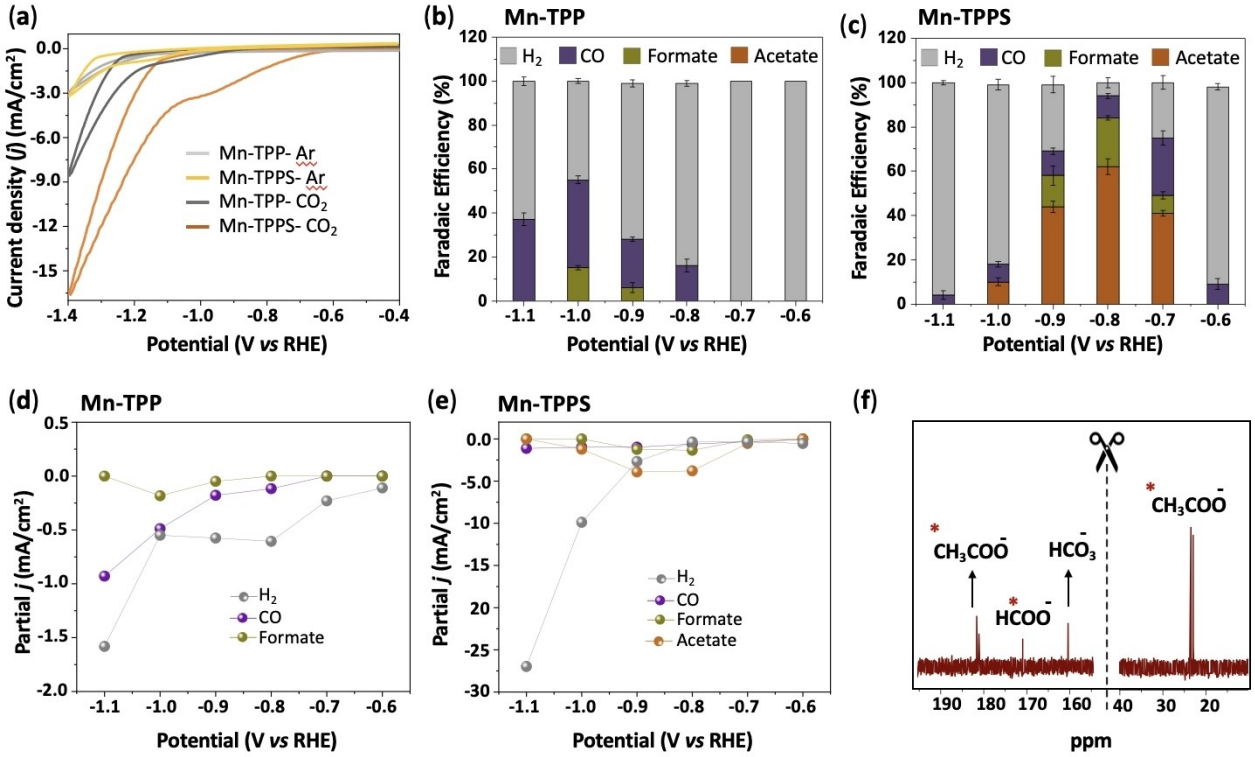

Figure 3. (a) Cyclic voltammetry (CV) comparison of electrografted Mn-TPP and Mn-TPPS under CO_2 and Ar in 0.1 M $KHCO_3$. Faradaic efficiency comparison of (b) Mn-TPP, and (c) Mn-TPPS at various potentials of −0.6 to −1.1 V vs. RHE in 0.1 M $KHCO_3$. Partial current density comparison of reducing CO_2 products using (d) Mn-TPP; and (e) Mn-TPPS. (f) ^{13}C NMR spectrum of the liquid products from electrocatalytic reduction reaction of Mn-TPPS under $^{13}CO_2/^{12}CO_2$ (1 : 1 ratio) at −0.8 V vs. RHE in 0.1 M $KHCO_3$ solution.

with CO_2 beginning at −0.9, and −0.6 V vs. RHE, respectively. This result highlights the importance of the sulfonate group in catalyzing CO_2RR at a lower overpotential owing to their electron-withdrawing properties group, which could facilitate the C–O bond cleavage.[57,58]

To determine the optimal potential for CO_2RR of this system, controlled constant potential electrolysis was attained for both Mn-TPP and Mn-TPPS using chronoamperometry at the constant potential of −0.6, −0.7, −0.8, −0.9, and −1.1 V vs. RHE (Figure S8). The current density increased linearly at more negative potentials as HER became more kinetically favored. The reduced gaseous products were periodically sampled from the cathodic chamber headspace and analyzed by gas chromatography (GC). Liquid products were analyzed using High-performance liquid chromatography (HPLC) and nuclear magnetic resonance (NMR) spectroscopy. H_2 and CO were the only gaseous products detected by GC, while formate and acetate were observed as liquid products.

Comparing the Faradaic efficiency of Mn-TPP at various potentials of −0.6 to −1.1 V vs. RHE, the highest catalytic activity was obtained at −1.0 V vs. RHE with the highest CO and formate selectivities (Figure 3b). At this potential, CO and formate were observed as the reduced products with the highest FE_{total} of 55% (FE_{CO}: 40%, $FE_{Formate}$: 15%) at the current density of −1.22 mA/cm^2. No acetate was observed at any applied potentials. In contrast, Mn-TPPS reacted differently (Figure 3c). CO production was first detected at −0.6 V vs. RHE. At a more negative potential of −0.7 V vs. RHE, formate and acetate were observed, which reached the maximum amount at −0.8 V vs. RHE, where acetate became the primary reduction product with the FE_{total}: 94% (FE_{CO}: 10%, $FE_{Formate}$: 22%, $FE_{Acetate}$: 62%) and current density of −6.1 mA/cm^2. The ability for Mn-TPPS to achieve a greater catalytic performance at a more positive potential indicates CO_2RR as the dominant catalytic pathway over HER compared to Mn-TPP under the same conditions highlighting the important role of the sulfonate group in improving the overall electrochemical activity.

The comparison of the partial current density of the reduced products for Mn-TPP (Figure 3d) and Mn-TPPS (Figure 3e) shows that Mn-TPPS produces a larger amount of reduced products. With a significant increase in acetate, the formation was observed at the optimal potential of −0.8 and −0.9 V vs. RHE. Achieving C_2 products using Mn-TPPS can be attributed to the orientation afforded by the negatively charged sulfonate groups – causing them to be perpendicular to the plane of the electrode. To evaluate the stability of Mn-TPPS, it was operated at −0.8 V vs. RHE for 6 hours, and we found that the selectivity of acetate was maintained with 3.2% degradation (Figure S10).

To verify the source of carbon in the products, we performed an isotopic labelling control experiment using $^{13}CO_2/^{12}CO_2$ (1 : 1 ratio) (Figure 3f and Figure S11). The ^{13}C NMR spectrum reveals two signals at 23 ppm and two at 181 ppm,

which belong to acetate, and one peak at 170 ppm belongs to formate, which verifies the presence of fully ^{13}C-labeled acetate and formate. Using proton NMR under $^{13}CO_2$ and $^{12}CO_2$ electrochemical reactions, the mixture of characteristic proton peaks assigned to acetate and formate was observed. The resulting ^{1}H NMR in Figure S12 shows the proton peak belonging to the methyl group of acetate (at 1.74 ppm) was symmetrically split into two peaks (at 1.59 and 1.91 ppm) in the case of using labelled $^{13}CO_2$ which is due to the large coupling constant between $^{13}CO_2$ and H.[59] The results are in agreement with previous reports.[36,59]

To elucidate the local electronic structure comparison of the Mn center in Mn-TPP and Mn-TPPS, the Mn K-edge X-ray absorption near-edge spectroscopy (XANES) was measured and reported in Figure 4, where the 'edge' refers to an absorption band generated by the promotion of a core electron to an unoccupied orbital and the oxidation state of the metal.[60,61] A large shift of 10–15 eV was observed in Mn-TPPS compared to Mn-TPP, which can be attributed to the electron-withdrawing effect of the sulfonate groups, affecting the electronic structure of the Mn in Mn-TPPS.

This could redistribute the electrons on the Mn site upon CO_2 adsorption, resulting in the transfer of electrons from the Mn center to 2p orbital of carbon in CO_2 to form a $CO_2^{\bullet-}$ species in the case of Mn-TPPS.[61,62] This result is in agreement with the reported in the literature.[63]

Mechanistic study

In this project, we successfully reduced CO_2 to CO, formate and acetate by engineering the molecular structure and surface topology of heterogeneous Mn-porphyrin-based electrocatalysts. A similar observation of the reduction of CO_2 to CO and $HCOO^-$ with metalloporphyrins has been reported previously.[36,64] In the current work, Mn-TPP and Mn-TPPS acting as metal-active porphyrin species possessing the ability to stabilize $*CO_2^{\bullet-}$ and consequently, reduce it to CO via 2 e^- transfer followed by the formation of acetate via 8 e^- transfer. Unlike non-substituted Mn-TPP, which only produces CO and H_2 with lower catalytic activity, Mn-TPPS showed increased catalytic activity at lower overpotential for CO_2RR electroreduction to both C_1 (CO and formate) and C_2 (acetate) products. This task was further evaluated through an operando IR thermography,[65] which confirms the higher activity of Mn-TPPS at a lower overpotential compared to Mn-TPP (Figure S15-S16, part S4).

Based on the earlier studies on Mn-complexes,[36,63,66,67] the manganese metal center undergoes one or two-electron reduction leading to the conversion of Mn^{II}/Mn^{III} to Mn^{I}/Mn^{II}, which reacts with CO_2 molecule. In the case of Fe and Mn porphyrin-like structures, although CO* is proposed to bind strongly enough to produce other C_1 products, the possibility for C–C coupling towards C_2 products from CO has been ignored.[68] Applying transitional metal centers in phthalocyanines has also shown a good selectivity towards CO formation, but the smaller energy gap between *CO and CO release eliminates the possibility for C–C coupling.[69] To gain further insight into the reaction mechanism and investigate the critical C–C coupling steps in the case of Mn-TPPS, DFT calculations were conducted. We consider *CO as an initial intermediate based on observing CO and acetate both as products. Two possible pathways could lead to C–C coupling and acetate formation (Figure 5a, Figure S15-S16). The first pathway involves the proton-coupled electron transfer (PCET) step to form *COH, followed by the addition of CO to create *COH–CO (*COH pathway). The second possible pathway involves a CO addition as the initial step, followed by a PCET step to *COH–CO (*COCO pathway). Once *COH–CO forms on the catalyst, it can undergo several PCET steps to form acetate.[70]

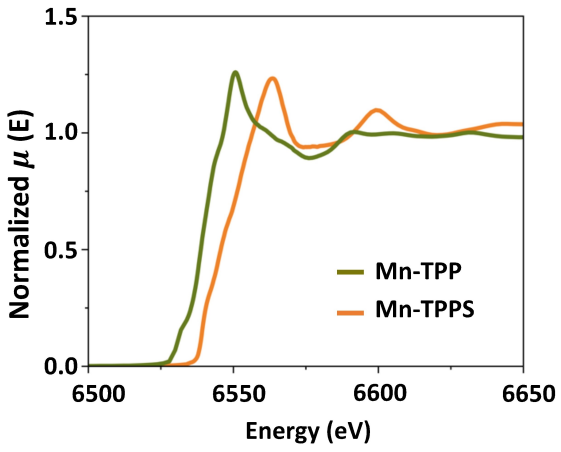

Figure 4. The Mn K-edge X-ray absorption near-edge spectroscopy (XANES) comparison of Mn-TPP and Mn-TPPS.

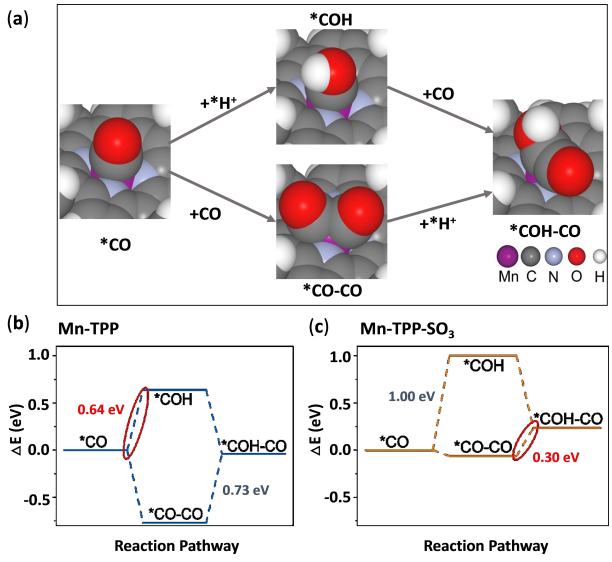

Figure 5. DFT investigation in C–C coupling on Mn-TPP and Mn-TPPS. a) geometries of two possible C–C coupling pathways towards C_2 product formation on Mn-TPPS. Energy calculations for two C–C coupling pathways on b) Mn-TPP and c) Mn-TPPS with the favored rate-determining steps highlighted in red circles.

With *CO as the starting point step and *COH–CO as the endpoint for our DFT study, the energy barriers for two possible C–C pathways were calculated on Mn-TPP (as control) and Mn-TPPS. Both Mn-TPP and Mn-TPPS showed similar binding geometries. As shown in Figures 5b and 5c, the PCET steps (*CO→*COH, *CO–CO→*COH–CO) are uphill in the energy on both Mn-TPP and Mn-TPPS, while CO addition steps (*CO→*CO–CO, *COH→*COH–CO) show downhill energy barriers. On Mn-TPP, *COH pathway has a lower energy barrier (0.64 eV) compared to *CO–CO pathway (0.73 eV). With the addition of SO_3^- functional groups on Mn-TPP, *CO–CO pathway exhibits the lowest energy barrier (0.30 eV), and *COH pathway has the highest energy barrier (1.00 eV). Based on our calculations, the presence of SO_3^- on Mn-TPP could lower the energy barrier from 0.64 eV to 0.30 eV, thus promoting C–C dimerization and leading to acetate formation. To our knowledge, our study is the first in the field to investigate the actual C–C coupling mechanism on Mn-based porphyrins catalysts. The revealed binding geometries as well as the effect from additional groups, can guide future work to design novel catalysts for generating high-value C_2 products.

Conclusion

In summary, our study demonstrates the importance of synthetic strategy for heterogeneous molecular electrocatalysts designed for CO_2RR. We have theoretically and experimentally investigated the influence of SO^{3-} substituents on the performance of Mn-porphyrin CO_2RR catalysts, immobilized via electrografting in an aqueous environment. The Mn-catalyst demonstrated an excellent FE at a low potential for the conversion of CO_2 to acetate. This enhancement in catalytic performance is owed to the electrostatic interaction of the SO_3^- group with water molecules, allowing higher surface coverages of the catalyst at an orientation more favorable for coupling processes. Another great advantage of this methodology is that the water-soluble TPPS, can serve as a heterogeneous catalyst in an aqueous solution through a strong porphyrin covalent bond with the electrode surface. Using heterogeneous hydrophilic compounds in aqueous environments opens a new approach to designing and optimizing next-generation heterogeneous electrocatalysts for CO_2RR. The focus of our current study was to show the potential of electrografting combined with molecular catalysts can produce high-value two-carbon products in an H-cell system which can be scaled up using GDEs and membrane electrode assembly (MEA) cells.

Acknowledgements

We gratefully acknowledge Bart Boshuizen for his support on the XPS study.

Conflict of Interest

The authors declare no conflict of interest.

Data Availability Statement

The data that support the findings of this study are available from the corresponding author upon reasonable request.

Keywords: CO_2RR · CO_2 to acetate · CO_2 electroreduction · manganese porphyrin · porphyrins

[1] C. Long, X. Li, J. Guo, Y. Shi, S. Liu, Z. Tang, *Small Methods* **2019**, *3*, 1800369.
[2] M. Li, E. Irtem, H.-P. Iglesias van Montfort, M. Abdinejad, T. Burdyny, *Nat. Commun.* **2022**, *13*, 5398.
[3] J. Wu, Y. Huang, W. Ye, Y. Li, *Adv. Sci.* **2017**, *4*, 1700194.
[4] S. Subramanian, K. Yang, M. Li, M. Sassenburg, M. Abdinejad, E. Irtem, J. Middelkoop, T. Burdyny, *ACS Energy Lett.* **2022**, 222–229.
[5] S. Liang, L. Huang, Y. Gao, Q. Wang, B. Liu, *Adv. Sci.* **2021**, *8*, 2102886.
[6] M. Abdinejad, M. K. Motlagh, M. Noroozifar, H. B. Kraatz, *Mater Adv* **2022**, *3*, 1224–1230.
[7] M. Abdinejad, C. Ferrag, M. N. Hossain, M. Noroozifar, K. Kerman, H. B. Kraatz, *J. Mater. Chem. A* **2021**, *9*, 12870–12877.
[8] M. Abdinejad, Z. Mirza, X. Zhang, H.-B. Kraatz, *ACS Sustainable Chem. Eng.* **2020**, *8*, 1715–1720.
[9] M. Li, K. Yang, M. Abdinejad, C. Zhao, T. Burdyny, *Nanoscale* **2022**, DOI 10.1039/D2NR03310K.
[10] E. Boutin, L. Merakeb, B. Ma, B. Boudy, M. Wang, J. Bonin, E. Anxolabéhère-Mallart, M. Robert, *Chem. Soc. Rev.* **2020**, *49*, 5772–5809.
[11] S. Zhang, Q. Fan, R. Xia, T. J. Meyer, *Acc. Chem. Res.* **2020**, *53*, 255–264.
[12] M. Abdinejad, M. N. Hossain, H.-B. Kraatz, *RSC Adv.* **2020**, *10*, 38013–38023.
[13] D. J. Hamilton, *Science* **2003**, *299*, 1702-1706.
[14] D. Grammatico, A. J. Bagnall, L. Riccardi, M. Fontecave, B.-L. Su, L. Billon, *Angew. Chem. Int. Ed.* **2022**, *61*, e202206399.
[15] M. Abdinejad, K. Tang, C. Dao, S. Saedy, T. Burdyny, *J. Mater. Chem. A* **2022**, *10*, 7626–7636.
[16] M. Abdinejad, E. Irtem, A. Farzi, M. Sassenburg, S. Subramanian, H.-P. I. van Montfort, D. Ripepi, M. Li, J. Middelkoop, A. Seifitokaldani, T. Burdyny, *ACS Catal.* **2022**, *12*, 7862–7876.
[17] M. Abdinejad, I. Santos da Silva, H. B. Kraatz, *J. Mater. Chem. A* **2021**, *9*, 9791–9797.
[18] E. Boutin, M. Robert, *Trends Chem.* **2021**, *3*, 359–372.
[19] H.-Q. Liang, T. Beweries, R. Francke, M. Beller, *Angew. Chem. Int. Ed.* **2022**, *61*, e202200723.
[20] D. Dedić, A. Dorniak, U. Rinner, W. Schöfberger, *Front. Chem.* **2021**, *9*, 540.
[21] M. Abdinejad, C. Dao, X. Zhang, H. B. Kraatz, *J. Energy Chem.* **2021**, *58*, 162–169.
[22] M. Abdinejad, C. Dao, B. Deng, F. Dinic, O. Voznyy, X. Zhang, H.-B. Kraatz, *ACS Sustainable Chem. Eng.* **2020**, *8*, 9549–9557.
[23] M. Abdinejad, C. Dao, B. Deng, M. E. Sweeney, F. Dielmann, X. Zhang, H. B. Kraatz, *ChemistrySelect* **2020**, *5*, 979–984.
[24] F. D'Souza, O. Ito, *Chem. Commun.* **2009**, 4913–4928.
[25] G. F. Manbeck, E. Fujita, *J. Porphyrins Phthalocyanines* **2015**, *19*, 45–64.
[26] X.-M. Hu, S. U. Pedersen, K. Daasbjerg, *Curr. Opin. Electrochem.* **2019**, *15*, 148–154.
[27] M. Abdinejad, A. Seifitokaldani, C. Dao, E. H. Sargent, X. A. Zhang, H. B. Kraatz, *ACS Appl. Energ. Mater.* **2019**, *2*, 1330–1335.
[28] I. Bhugun, D. Lexa, J. M. Savéant, *J. Am. Chem. Soc.* **1996**, *118*, 1769–1776.
[29] X. M. Hu, M. H. Rønne, S. U. Pedersen, T. Skrydstrup, K. Daasbjerg, *Angew. Chem. Int. Ed.* **2017**, *56*, 6468–6472; *Angew. Chem.* **2017**, *129*, 6568–6572.
[30] M. Zhu, J. Chen, L. Huang, R. Ye, J. Xu, Y.-F. Han, *Angew. Chem. Int. Ed.* **2019**, *58*, 6595–6599; *Angew. Chem.* **2019**, *131*, 6667–6671.

[31] M. Usman, M. Humayun, M. D. Garba, L. Ullah, Z. Zeb, A. Helal, M. H. Suliman, B. Y. Alfaifi, N. Iqbal, M. Abdinejad, A. A. Tahir, H. Ullah, *Nanomaterials* **2021**, *11*, DOI 10.3390/nano11082029.
[32] M. Abdinejad, L. F. B. Wilm, F. Dielmann, H. B. Kraatz, *ACS Sustainable Chem. Eng.* **2021**, *9*, 521–530.
[33] Y. Wu, J. Jiang, Z. Weng, M. Wang, D. L. J. Broere, Y. Zhong, G. W. Brudvig, Z. Feng, H. Wang, *ACS Cent. Sci.* **2017**, *3*, 847–852.
[34] W. Ju, A. Bagger, G.-P. Hao, A. S. Varela, I. Sinev, V. Bon, B. Roldan Cuenya, S. Kaskel, J. Rossmeisl, P. Strasser, *Nat. Commun.* **2017**, *8*, 944.
[35] F. Pan, W. Deng, C. Justiniano, Y. Li, *Appl. Catal. B* **2018**, *226*, 463–472.
[36] R. De, S. Gonglach, S. Paul, M. Haas, S. S. Sreejith, P. Gerschel, U.-P. Apfel, T. H. Vuong, J. Rabeah, S. Roy, W. Schöfberger, *Angew. Chem. Int. Ed.* **2020**, *59*, 10527–10534; *Angew. Chem.* **2020**, *132*, 10614–10621.
[37] A. N. Marianov, Y. Jiang, *ACS Sustainable Chem. Eng.* **2019**, *7*, 3838–3848.
[38] E. Frackowiak, F. Béguin, *Carbon* **2001**, *39*, 937–950.
[39] I. Willerich, H. Ritter, F. Gröhn, *J. Phys. Chem. B* **2009**, *113*, 3339–3354.
[40] I. Azcarate, C. Costentin, M. Robert, J.-M. Savéant, *J. Am. Chem. Soc.* **2016**, *138*, 16639–16644.
[41] C. Costentin, J. M. Savéant, *Nat. Chem. Rev.* **2017**, *1*, 1–8.
[42] G. Z. G. Meng, B. R. James, K. a. Skov, *Can. J. Chem.* **1994**, *72*, 1894–1909.
[43] W. J. Krupei, T. A. Chamberlin, M. Kochanny, *J. Org. Chem.* **1989**, *54*, 2753–2756.
[44] R. Luguya, L. Jaquinod, F. R. Fronczek, M. G. H. Vicente, K. M. Smith, *Tetrahedron* **2004**, *60*, 2757–2763.
[45] R. Rubires, J. Crusats, Z. El-Hachemi, T. Jaramillo, M. López, E. Valls, J.-A. Farrera, J. M. Ribó, *New J. Chem.* **1999**, *23*, 189–198.
[46] J. P. Collman, P. S. Wagenknecht, J. E. Hutchison, *Angew. Chem. Int. Ed. Engl.* **1994**, *33*, 1537–1554.
[47] L. Bajema, M. Gouterman, B. Meyer, *J. Mol. Spectrosc.* **1968**, *27*, 225–235.
[48] S. Phal, K. Shimizu, D. Mwanza, P. Mashazi, A. Shchukarev, S. Tesfalidet, *Mol.* **2020**, *25*, DOI 10.3390/molecules25194575.
[49] J. Agullo, M. Morin, D. Bélanger, *J. Electrochem. Soc.* **2012**, *159*, H758–H764.
[50] A. N. Marianov, Y. Jiang, *Appl. Catal. B* **2019**, *244*, 881–888.
[51] R. D. Rocklin, R. W. Murray, *J. Electroanal. Chem. Interfacial Electrochem.* **1979**, *100*, 271–282.
[52] M. Li, W. Lei, Y. Yu, W. Yang, J. Li, D. Chen, S. Xu, M. Feng, H. Li, *Nanoscale* **2018**, *10*, 15926–15931.
[53] M. Paszkiewicz, T. Biktagirov, H. Aldahhak, F. Allegretti, E. Rauls, W. Schöfberger, W. G. Schmidt, J. V. Barth, U. Gerstmann, F. Klappenberger, *J. Phys. Chem. Lett.* **2018**, *9*, 6412–6420.
[54] T. Menanteau, E. Levillain, A. J. Downard, T. Breton, *Phys. Chem. Chem. Phys.* **2015**, *17*, 13137–13142.
[55] Z. Peng, Z. Jiang, X. Huang, Y. Li, *RSC Adv.* **2016**, *6*, 13742–13748.
[56] A. Shafaei Douk, H. Saravani, M. Z. Yazdan Abad, M. Noroozifar, *ACS Appl. Energ. Mater.* **2020**, *3*, 7527–7534.
[57] C. H. Lim, A. M. Holder, J. T. Hynes, C. B. Musgrave, *J. Am. Chem. Soc.* **2014**, *136*, 16081–16095.
[58] M. Lessio, E. A. Carter, *J. Am. Chem. Soc.* **2015**, *137*, 13248–13251.
[59] X.-F. Qiu, J.-R. Huang, C. Yu, Z.-H. Zhao, H.-L. Zhu, Z. Ke, P.-Q. Liao, X.-M. Chen, *Angew. Chemie Int. Ed.* **2022**, *n/a*, e202206470.
[60] D. C. Koningsberger, R. Prins, **1987**.
[61] E. Fujita, L. R. Furenlid, M. W. Renner, *J. Am. Chem. Soc.* **1997**, *119*, 4549–4550.
[62] J. Feng, H. Gao, L. Zheng, Z. Chen, S. Zeng, C. Jiang, H. Dong, L. Liu, S. Zhang, X. Zhang, *Nat. Commun.* **2020**, *11*, 4341.
[63] B. Zhang, J. Zhang, J. Shi, D. Tan, L. Liu, F. Zhang, C. Lu, Z. Su, X. Tan, X. Cheng, B. Han, L. Zheng, J. Zhang, *Nat. Commun.* **2019**, *10*, 2980.
[64] A. J. Göttle, M. T. M. Koper, *J. Am. Chem. Soc.* **2018**, *140*, 4826–4834.
[65] H.-P. Iglesias van Montfort, T. Burdyny, *ACS Energy Lett.* **2022**, *7*, 2410–2419.
[66] J. J. Walsh, C. L. Smith, G. Neri, G. F. S. Whitehead, C. M. Robertson, A. J. Cowan, *Faraday Discuss.* **2015**, *183*, 147–160.
[67] I. Hod, M. D. Sampson, P. Deria, C. P. Kubiak, O. K. Farha, J. T. Hupp, *ACS Catal.* **2015**, *5*, 6302–6309.
[68] A. Bagger, W. Ju, A. S. Varela, P. Strasser, J. Rossmeisl, *Catal. Today* **2017**, *288*, 74–78.
[69] Q. Chang, Y. Liu, J.-H. Lee, D. Ologunagba, S. Hwang, Z. Xie, S. Kattel, J. H. Lee, J. G. Chen, *J. Am. Chem. Soc.* **2022**, *144*, 16131–16138.
[70] P. Zhu, C. Xia, C.-Y. Liu, K. Jiang, G. Gao, X. Zhang, Y. Xia, Y. Lei, H. N. Alshareef, T. P. Senftle, H. Wang, *Proc. Nat. Acad. Sci.* **2021**, *118*, e2010868118.

Manuscript received: December 20, 2022
Accepted manuscript online: December 28, 2022
Version of record online: February 3, 2023